nature physics

Article

https://doi.org/10.1038/s41567-023-01948-1

Transition from a polaronic condensate to a degenerate Fermi gas of heteronuclear molecules

Received: 28 July 2022

Accepted: 6 January 2023

Published online: 13 February 2023

Check for updates

Marcel Duda[1,2], Xing-Yan Chen[1,2], Andreas Schindewolf[1,2], Roman Bause[1,2], Jonas von Milczewski[1,2], Richard Schmidt[1,2,3,4], Immanuel Bloch[1,2,5] & Xin-Yu Luo[1,2]

The interplay of quantum statistics and interactions in atomic Bose–Fermi mixtures leads to a phase diagram markedly different from pure fermionic or bosonic systems. However, investigating this phase diagram remains challenging when bosons condense due to the resulting fast interspecies loss. Here we report observations consistent with a phase transition from a polaronic to a molecular phase in a density-matched degenerate Bose–Fermi mixture. The condensate fraction, representing the order parameter of the transition, is depleted by interactions, and the build-up of strong correlations results in the emergence of a molecular Fermi gas. The features of the underlying quantum phase transition represent a new phenomenon complementary to the paradigmatic Bose–Einstein condensate/Bardeen–Cooper–Schrieffer crossover observed in Fermi systems. By driving the system through the transition, we produce a sample of sodium–potassium molecules exhibiting a large molecule-frame dipole moment in the quantum-degenerate regime.

Mixtures of interacting bosons and fermions have been the subject of intense research since conventional superconductivity was understood to arise from the effective attraction between electrons mediated by phonons. In solid-state materials, the electron–phonon coupling is captured by Fröhlich or Holstein models. Developments in ultracold atoms[1] and van der Waals materials[2] now make it possible to realize Bose–Fermi mixtures that are governed by beyond-Fröhlich physics where bosons and fermions can bind to fermionic molecules[3–8] reaching the quantum-degenerate regime[9]. The competition between this novel bound state physics and mediated interactions leads to an enriched phase diagram potentially featuring supersolidity and charge-density-wave phases[10–13], molecular Fermi liquids[14–19] and unconventional boson-induced superconductivity[20,21].

Experimentally, the phase diagram of Bose–Fermi mixtures has primarily been explored in the regime of large population imbalance where one species acts as a dilute, thermal gas of impurities dressed by its environment. Bose polarons were recently observed in the limit of fermionic impurities in a bosonic bath[22–24], while the existence of a transition from Fermi polarons to molecules has by now been firmly established for impurities immersed in a Fermi sea[25–28]. However, it has remained unclear how the transition from atoms to molecules proceeds when the impurities are degenerate, in particular when bosons and fermions of comparable density dress each other mutually and drastically modify their respective behaviour. Importantly, this regime of matched particle density is promising for the association of heteronuclear molecules at high phase space density, which finds wide-ranging applications in quantum chemistry and the exploration of dipolar quantum many-body systems[29,30]. At the same time, reaching this regime is notoriously difficult in double-degenerate mixtures due to the enhanced density of the bosonic condensate. The excess density

[1]Max-Planck-Institut für Quantenoptik, Garching, Germany. [2]Munich Center for Quantum Science and Technology, München, Germany. [3]Center for Complex Quantum Systems, Department of Physics and Astronomy, Aarhus University, Aarhus, Denmark. [4]Institute for Theoretical Physics, Heidelberg University, Heidelberg, Germany. [5]Fakultät für Physik, Ludwig-Maximilians-Universität, München, Germany. e-mail: xinyu.luo@mpq.mpg.de

https://doi.org/10.1038/s41567-023-01948-1

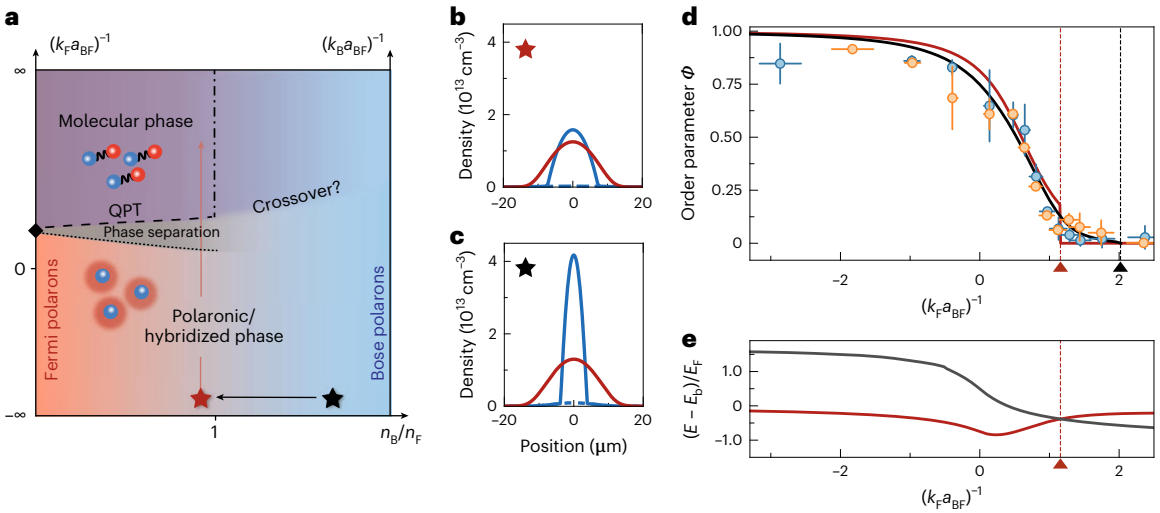

Fig. 1 | QPT in a density-matched Bose–Fermi mixture. a, Phase diagram of degenerate Bose–Fermi mixtures as a function of the density ratio n_B/n_F and the dimensionless interaction strength $(k_i a_{BF})^{-1}$. For $n_B/n_F \to 0$ one attains the Fermi polaron limit, featuring a polaron-to-molecule transition (black diamond), whereas for $n_B/n_F \to \infty$, the Bose polaron limit with a smooth crossover is reached. For $n_B < n_F$, a QPT between a polaronic and a molecular phase of either first order with phase separation or second order is expected. The long-dashed line marks the complete depletion of the condensate $(k_F a_{BF})_c^{-1}$ and, in the case of phase separation, the dotted line marks its onset at $(k_F a_{BF})_{ps}^{-1}$. The dash-dotted line marks a possible further QPT of unknown order. **b**,**c**, Calculated in situ density profiles of bosons (blue) and fermions (red) in the species-dependent 785-nm dipole trap (**b**) and in the far-detuned trap (**c**) (Methods). The dashed blue line gives the thermal boson fraction, showing a lack of thermal bosons in regions where bosons and fermions overlap. **d**, Order parameter ϕ as a function of $(k_F a_{BF})^{-1}$ for the boson–fermion average-density ratio $\bar{n}_B/\bar{n}_F = 0.4$ (orange points) and $\bar{n}_B/\bar{n}_F = 0.7$ (blue points). The error bars are discussed in Methods. The black solid line shows the order parameter from zero-temperature theory in ref. [18], predicting the QPT to occur at $(k_F a_{BF})_c^{-1} = 2.02$ (black triangle) for ideal bosons interacting with a Fermi gas at $n_B/n_F = 1$. The red solid line shows the polaron quasiparticle weight of a bosonic impurity in a Fermi gas obtained from a self-consistent fRG calculation that predicts the polaron-to-molecule transition to occur at $(k_F a_{BF})_c^{-1} = 1.16$ (red triangle). **e**, Energy spectrum of the zero-momentum Fermi polaron (red line) and the zero-momentum molecule (grey line) for a single bosonic impurity obtained from the fRG. The energies cross at the polaron-to-molecule transition (red dashed line). For $a_{BF} > 0$, the binding energy $E_b = -\hbar^2/2\mu a_{BF}^2$ is subtracted, where μ is the reduced mass.

of the Bose–Einstein condensate (BEC) causes fast interspecies loss, which remains the key bottleneck for reaching quantum degeneracy in heteronuclear molecules and for the study of strongly correlated Bose–Fermi mixtures.

In this Article we investigate strongly interacting Bose–Fermi mixtures with comparable densities. Our data suggest that, in the low-temperature regime where the bosonic impurities condense, strong boson–fermion interactions induce a phase transition from a polaronic condensate to a molecular Fermi gas, connecting to an underlying quantum phase transition (QPT) at $T = 0$ (ref. [16]). Using a novel density-decompression technique that mitigates atomic loss, we produce a double-degenerate Bose–Fermi mixture of ^{23}Na and ^{40}K with matched density and reveal signatures of this QPT. Starting from a weakly interacting mixture, increased attractive interactions dress the bosonic condensate polaronically. By continuously tuning the interaction strength, the polaronic condensate is depleted and a transition into a phase of quantum-degenerate fermionic molecules is observed. Driving the underlying QPT enhances the association efficiency of Feshbach molecules to near unity. This enables the subsequent creation of ground-state ^{23}Na^{40}K molecules with a large molecular-frame dipole moment of 2.7 debye in the quantum-degenerate regime.

Degenerate Bose–Fermi mixtures in density-matched regime

A simplified phase diagram of Bose–Fermi mixtures is illustrated in Fig. 1a as a function of the ratio of boson to fermion density n_B/n_F and the dimensionless interaction strength $1/k_i a_{BF}$. Here, a_{BF} denotes the boson–fermion scattering length, and the wavevector k_i is determined by the interparticle spacing of the majority species $k_i = (6\pi^2 n_i)^{1/3}$, where i denotes B(F) for $n_B > n_F$ ($n_B < n_F$). Phases involving bound states of more than one boson are ignored, as these are intrinsically unstable due to fast recombination loss.

Qualitatively, the phase diagram in Fig. 1a can then be divided into two regimes. In the limit of vanishing Bose–Fermi attraction, $(k_i a_{BF})^{-1} \to -\infty$, bosons and fermions decouple and form a BEC along with a Fermi sea. As attractive interactions are switched on, fermions and bosons modify each other's properties, leading to quasiparticle formation. Due to the polaronic character of this interaction, we denote the resulting phase as the 'polaronic phase'. In the opposite limit of strong attraction, realized at $(k_i a_{BF})^{-1} \to \infty$, for $n_B \leq n_F$, binding of all bosons to fermions leads to a Fermi sea of molecules coexisting with an atomic Fermi sea, and we denote this phase the 'molecular phase'. For $n_B \leq n_F$, the polaronic and molecular phase are predicted to be either separated by a first-order QPT with phase separation or by a second-order QPT[14,16–18,31,32]. When tuning the density ratio across $n_B/n_F \approx 1$ in the regime of strong attraction, an additional phase transition, where a condensate reappears, is predicted to occur[14]. This phase featuring molecules and an excess condensate is predicted to cross over into the polaronic phase for $n_B/n_F \gtrsim 1$ (ref. [14]). Most experiments have been carried out in the impurity limits either on the far left-hand or the far right-hand side of the phase diagram[22,24–28].

A natural way to investigate the phase diagram away from the impurity limits starts from producing a double-degenerate Bose–Fermi mixture. The regime of matched densities is of particular interest, where the system becomes strongly correlated and neither of the atomic species can be regarded as a quantum impurity. To access this novel regime, we employ a species-dependent dipole trap at 785 nm, which is near-detuned to the D-lines of the K atoms. This trap provides a weaker confinement of the Na atoms compared to the K atoms, lowering the density of the Na BEC and increasing overlap between the species (Fig. 1b). As a consequence, the detrimental loss resulting

https://doi.org/10.1038/s41567-023-01948-1

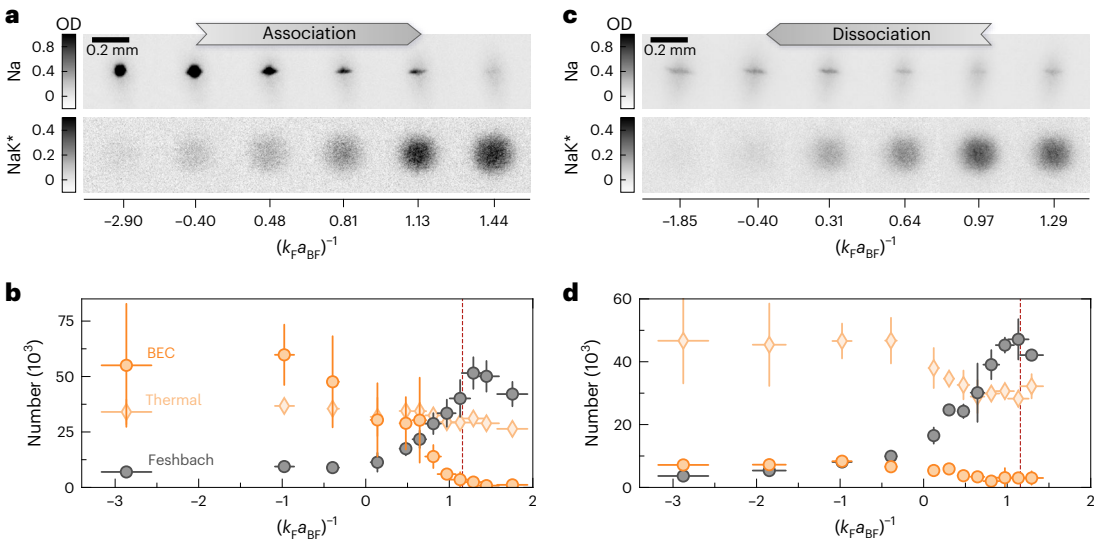

Fig. 2 | Association and dissociation process of degenerate Feshbach molecules. a, Absorption images showing the optical density (OD) of Na atoms (Na) and Feshbach molecules (NaK*) after 18-ms time of flight during the association ramp from the polaronic BEC to the molecular phase. **b**, Production of Feshbach molecules. Numbers of condensed Na atoms (dark orange points), thermal Na atoms (bright orange diamonds) and Feshbach molecules (grey points) are shown as a function of $(k_F a_{BF})^{-1}$ for $\bar{n}_B/\bar{n}_F = 0.7$. The red dashed line in **b** and **d** indicates the polaron-to-molecule transition at $(k_F a_{BF})^{-1} = 1.16$ in the Fermi polaron problem. **c**, Absorption images during the dissociation ramp with 18-ms time of flight. **d**, Dissociation of Feshbach molecules. Condensed Na atom (dark orange points), thermal Na atom (bright orange diamonds) and Feshbach molecule (grey points) numbers are shown as a function of $(k_F a_{BF})^{-1}$ for $\bar{n}_B/\bar{n}_F = 0.7$. The error bars are discussed in Methods.

from collisions of Na atoms in the BEC with NaK* Feshbach molecules is dramatically reduced (Methods). In contrast, for a typical trap set-up where the trapping effect is similar for both atomic species, the peak density of the BEC is considerably larger than that of the Fermi gas (Fig. 1c). This results in an entirely different physical regime related to the Bose polaron problem with a low molecule association efficiency when starting from the BEC (Methods).

QPT from a polaronic phase to a molecular phase

In the regime where $n_B \leq n_F$, theory at low temperature predicts a transition from a phase where a BEC coexists with a Fermi gas to a liquid where all bosons are bound into molecules[14,16–18,31,32]. By tuning the interactions from weak to strong coupling, the boson–fermion interaction gradually depletes the BEC until the condensate fraction, representing the order parameter of the transition, vanishes at the critical interaction parameter $(k_F a_{BF})_c^{-1}$, resulting in a phase transition. At this interaction strength for $T = 0$, a QPT occurs, possibly masked by a phase-separation regime[17,31,32]. This is a distinct feature in Bose–Fermi mixtures that is absent for the BEC/Bardeen–Cooper–Schrieffer (BEC-BCS) crossover in spin-balanced fermionic mixtures where no symmetry-breaking pattern is changed as the interaction strength is varied across the Feshbach resonance[33]. Furthermore, in contrast to the BEC-BCS phase, the molecular phase is more robust with respect to temperature[16,34,35]. In both cases, pairing is required, which is not affected by small temperature fluctuations, as pairing occurs with binding energies on the order of several Fermi energies. In the BEC-BCS phase, however, molecules are additionally required to condense, whereas in Bose–Fermi mixtures they merely need to form a Fermi sea.

The order of the transition depends on the Bose–Bose repulsion a_{BB} and the density ratio n_B/n_F (refs. [17,31,32]). The transition is predicted to be of first order in a large parameter regime, and only beyond a threshold do stronger Bose–Bose repulsion and lower n_B/n_F favour a second-order transition[17,32]. Tuning the Bose–Fermi interaction strength $(k_F a_{BF})^{-1}$ from weak to strong interactions at a fixed density ratio $n_B/n_F < 1$, the condensate density decreases smoothly and vanishes beyond a critical interaction parameter $(k_F a_{BF})_c^{-1}$ for a second-order phase transition. For a first-order transition, on the other hand, the homogeneous system passes through a phase-separation region. On reaching the lower boundary $(k_F a_{BF})_{ps}^{-1}$, the system enters a phase-separated state (Fig. 1a), where the local condensate density drops to zero discontinuously in some parts of the system, but remains finite in others. Tuning the interactions further, the mixing ratio between the two phases shifts towards the molecular phase and, once $(k_F a_{BF})_c^{-1}$ is reached, all parts of the system have transitioned to the molecular phase. Importantly, however, the globally averaged condensate density is expected to decrease smoothly and to vanish continuously at $(k_F a_{BF})_c^{-1}$ in both cases. This effect is enhanced by the harmonic trap (Fig. 1b,c), and it makes distinguishing between the two cases challenging.

Within the condensed polaronic phase it is predicted that the depletion of the condensate depends weakly on the boson–fermion density ratio, which, remarkably, extends all the way to the Fermi polaron limit, $n_B/n_F \to 0$ (refs. [18,28]). In the extreme limit of a single bosonic impurity in a Fermi gas, the phase transition connects to a polaron-to-molecule transition, and the condensate fraction reduces to the impurity quasiparticle weight (for a detailed explanation, see ref. [18]). A computational, self-consistent functional renormalization group (fRG) technique that takes into account an infinite number of particle–hole excitations of the Fermi sea (Methods)[36] predicts this transition to occur at $(k_F a_{BF})^{-1} = 1.16$ (Fig. 1e). This transition point is expected to shift to larger values as temperature and boson density increase[18,27,37].

In the following, we probe signatures of this QPT. Our experiment typically starts with 2.3×10^5 ^{40}K atoms at $T = 80$ nK (corresponding to $T/T_F \approx 0.2$, where T_F is the Fermi temperature) and 0.8×10^5 ^{23}Na atoms with a condensate fraction of 60% at a magnetic field of 81 G. We employ a single magnetic field ramp with a speed of 3.5 G ms^{-1} (Methods) that is terminated at the desired magnetic field close to a Feshbach resonance at 78.3 G (refs. [38,39]), corresponding to different interaction strengths $(k_F a_{BF})^{-1}$, while the Bose–Bose interaction remains at $a_{BB} = 53 a_0$ (ref. [38]). Due to the small effective-range parameter $k_F R^* = 0.08$ of this broad Feshbach resonance, the Bose–Fermi

https://doi.org/10.1038/s41567-023-01948-1

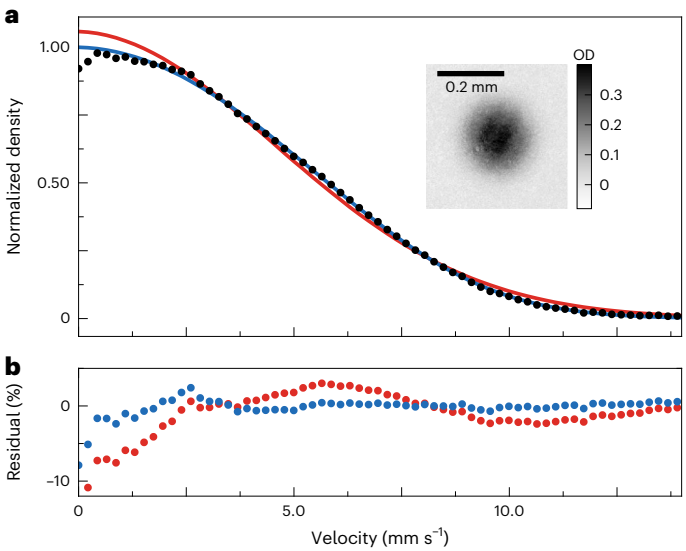

Fig. 3 | Quantum degeneracy of Feshbach molecules. a, Velocity distribution of Feshbach molecules. The angular integral (black points) of an average of 15 images with a time of flight of 15 ms (shown in the inset) was fitted with Fermi–Dirac (blue line) and Gaussian (red line) distributions. Although the Gaussian fit overestimates the occupation at lower velocities, the data are well described by a Fermi–Dirac distribution, which accounts for the Pauli blocking. The fit of the Fermi–Dirac distribution results in $T/T_F = 0.28(1)$. **b**, Angular integral of the residuals.

interactions are characterized by the single parameter $(k_F a_{BF})^{-1}$(Methods and ref. [38]). Throughout the magnetic field ramp, no collapse or immiscibility of the Bose–Fermi mixture are observed on the timescale of the experiment (Methods). Furthermore, we checked that the depletion of the BEC is independent of the ramp speed for the sufficiently slow ramp used here (Methods). This indicates that the system stays close to a local equilibrium state until near the critical point. We then quench the magnetic field to 72.3 G. This projects the system onto free atoms and deeply bound molecules, which are subsequently imaged in time of flight after Stern–Gerlach separation, as shown in Fig. 2a,b.

To characterize the phase transition quantitatively, we define the normalized order parameter $\phi = N_{BEC}/(N_m + N_{BEC})$. Here N_{BEC} and N_m represent the number of condensed Na atoms and those associated to molecules, respectively. The order parameter ϕ describes the depletion of the condensate fraction due to the excitation of bosons to finite-momentum states by quantum fluctuations. These quantum fluctuations are dominated by the build-up of pairing correlations, measured by the projection onto molecules. Note that, in the definition of ϕ, we disregard thermal Na atoms as we describe the condensate fraction in the centre of the trap. First, the spatial extension of thermal bosons (Fig. 1b) is much larger than that of the BEC and the fermions, both of which are concentrated in the centre of the trap. Here the density of thermal bosons is more than 20 times smaller than that of the BEC. Second, on the timescales of the experiment, thermal bosons do not play a significant role in molecule formation due to their weak spatial overlap with the fermions. Molecules are thus formed predominantly from BEC atoms.

The temperature of bosons in the centre of the trap where most of the boson–fermion collisions take place is thus effectively much lower than suggested by the equilibrium temperature, allowing us to directly compare our findings with zero-temperature theory. Specifically, in Fig. 1d we make a comparison with the quasiparticle weight of a bosonic impurity calculated from a self-consistent fRG approach (Methods)[36] (red dashed line) and predictions of the condensate fraction from a non-self-consistent T-matrix (NSCT) theory[18] (black solid line) for $n_B = n_F$ that neglects multiple particle–hole excitations in the Fermi sea.

In Fig. 1d, we show the measured order parameter ϕ as a function of $(k_F a_{BF})^{-1}$ for $\bar{n}_B/\bar{n}_F = 0.4$ and 0.7, where $\bar{n}_B/\bar{n}_F$ denotes the ratio of the average boson and fermion densities in parts of the trap with a finite condensate fraction in the weakly interacting regime. As the interaction strength increases, ϕ reduces slowly for $(k_F a_{BF})^{-1} < 0$. However, once the scattering length becomes positive, ϕ decreases rapidly and vanishes in the regime beyond $(k_F a_{BF})^{-1} = 1.44(15)$ $(\bar{n}_B/\bar{n}_F = 0.7)$ and $(k_F a_{BF})^{-1} = 1.75(18)(\bar{n}_B/\bar{n}_F = 0.4)$, where the residual condensate fraction is comparable to the uncertainty of the measurement. Our measurements agree well with the predicted condensate fraction from the NSCT approach throughout the entire interaction regime. Importantly, both datasets overlap within error bars, providing support for the predicted universality of the condensate depletion with respect to varying n_B/n_F (refs. [18,28]). This, in turn, justifies comparing our in-trap experiment with predictions for a homogeneous system. The data also show a remarkable agreement with the quasiparticle weight of a single impurity in most of the interaction regime, except close to the phase transition. This indicates that, despite having a large boson density, the system can be well described as a condensate of polaronically dressed bosons. In contrast, however, at the transition, the order parameter vanishes smoothly compared to a jump predicted in the impurity limit.

To estimate the transition point independently from the slowly varying order parameter, we consider the projected Feshbach molecule number shown in Fig. 2b as a measure of existing boson–fermion pairing correlations (Methods). As $(k_F a_{BF})^{-1}$ increases, so do the pairing correlations (including potential fermion–molecule mixing[14]), until they saturate when the bosons are fully bound into molecules. The resulting transition point $(k_F a_{BF})^{-1} = 1.29(14)$extracted from the measured Feshbach molecule number is consistent with the transition point obtained through the vanishing of the order parameter.

Driving through the transition provides an efficient method to create molecules. Our data show that a striking conversion efficiency of ~80% of the Na atoms in the BEC into Feshbach molecules can be achieved. Accounting for the residual density mismatch and the resulting interspecies loss from the excess bosons, our data suggest that the entirety of the BEC could be converted into molecules for perfectly matched density conditions. In contrast, the highest conversion efficiency from a BEC previously reported was less than 50% in KRb, where the density of bosons in the centre of the trap was ten times higher than that of the fermions, which was possible only because of the tenfold lower interspecies loss coefficients compared to NaK[9,39,40].

Next, we investigate the reversal of the phase transition. After the association ramp reaches $(k_F a_{BF})^{-1} = 1.3$, the magnetic field is ramped back to dissociate the molecules. The dissociation ramp is again followed by a magnetic-field quench to 72.3 G for detection. As can be seen from the time-of-flight images in Fig. 2c, the number of projected Feshbach molecules decreases, and a finite BEC fraction is recovered. In particular, we show that the number of Na atoms in the BEC can be increased from $3(2) \times 10^3$ to $8(1) \times 10^3$ (Fig. 2d). Heating is evident after the dissociation in the form of an increase of thermal Na atoms, which we attribute to the non-adiabatic nature of the magnetic-field ramps near the transition point. Due to the changing number of Na atoms in the thermal wings, we thus cannot characterize the reversal of the phase transition with the order parameter ϕ as done in the association ramp. Nonetheless, the partial restoration of the BEC highlights the coherence preserved in our experiment and is a striking example of how bosons that were bound into fermionic molecules in finite-momentum states are converted back into their motional ground state. Thus, the Fermi degeneracy of the molecules and the partial restoration of the BEC underline the low entropy of our molecular clouds.

Degenerate Fermi gas of NaK* Feshbach molecules

After the preparation 5×10^4 Feshbach molecules at a temperature of 100 nK by ramping across the QPT, we convert them to more deeply bound states by quenching the magnetic field to 75 G. At this magnetic field, we turn on a strong gradient to levitate the molecules and remove any residual atoms from the trap (Methods). Inelastic collisions between molecules are strongly suppressed by Pauli blocking, leading to a second-long lifetime (Methods). The quantum degeneracy of the molecular gas after association is determined by time-of-flight imaging after holding the molecules for 100 ms (Fig. 3), ensuring that collective oscillations induced by the magnetic-field ramps of the molecular cloud are dampened out (Methods). The momentum distribution of the molecules is well described by a Fermi–Dirac distribution[9] with a temperature of $T = 0.28(1)T_F$.

Low-entropy NaK ground-state molecules

The establishment of a means to efficiently create large ensembles of heteronuclear Feshbach molecules sets the stage for the creation of polar ground-state molecules. To achieve this, we coherently transfer the degenerate Fermi gas of 5×10^4 Feshbach molecules into the rovibronic ground state of the $X^1\Sigma^+$ electronic manifold[41], with an overall efficiency of up to 60%. The momentum distribution is maintained during the transfer and is still fit well by a Fermi–Dirac distribution at a temperature of $T = 0.28(3)T_F$. However, due to the absence of thermalization and the imperfect transfer efficiency, random holes are created in the molecular Fermi sea. Accordingly, we expect the quantum degeneracy of the ground-state molecular gas to be reduced compared to the Feshbach molecular gas[9,42]. Hence, as an alternative measure of the degeneracy, we compute the peak occupancy of the Fermi gas f, characterizing the probability of the lowest energy state in the Fermi gas to be occupied. Based on the transfer efficiency to the ground state and the initial degeneracy of the Feshbach molecules, we obtain a peak occupancy of $f = 57(3)\%$, which corresponds to an effective temperature of $T = 0.52(2)T_F$.

Conclusion

Using a species-dependent decompression technique of atomic clouds, we have observed signatures of a QPT in Bose–Fermi mixtures between a phase featuring condensation and a molecular Fermi gas, in excellent quantitative agreement with theory. By driving the system through this phase transition, we have produced a gas of quantum-degenerate Feshbach molecules with record efficiency. The characterized phase transition represents a new phenomenon complementary to the paradigmatic BEC-BCS crossover observed in Fermi systems[33] and the atomic-to-molecular BEC crossover in Bose systems[43]. It is a first step in the exploration of strong-correlation physics in degenerate Bose–Fermi systems and provides a benchmark for their theoretical understanding. The investigation of the order of the transition is an intriguing avenue for future research, such as an observation of hysteresis[17] and quantum critical dynamics[44] or the exploration of solid-state systems where chemical potentials can be readily tuned[2]. Our method can be extended to other Bose–Fermi mixtures for producing large degenerate samples of fermionic molecules and may help to achieve a heteronuclear molecular BEC from Bose–Bose mixtures, which suffer from even more severe losses when both bosonic species condense[45–50]. Ultimately, our technique allows us to produce a gas of non-reactive ground-state molecules in the quantum-degenerate regime with five times stronger molecular-frame dipole moments than the first degenerate polar molecules of KRb, and provides excellent conditions for evaporative cooling of ground-state molecules, as demonstrated for KRb[51,52] and recently also for NaK[53]. This opens up exciting opportunities to study strongly correlated dipolar quantum systems[54] ranging from the collapse of dipolar Fermi gases[55] to extended Heisenberg XXZ models[56] and extended Fermi–Hubbard models[57] in optical lattices.

Online content

Any methods, additional references, Nature Portfolio reporting summaries, source data, extended data, supplementary information, acknowledgements, peer review information; details of author contributions and competing interests; and statements of data and code availability are available at https://doi.org/10.1038/s41567-023-01948-1.

References

1. Chin, C., Grimm, R., Julienne, P. & Tiesinga, E. Feshbach resonances in ultracold gases. *Rev. Mod. Phys.* **82**, 1225–1286 (2010).
2. Sidler, M. et al. Fermi polaron-polaritons in charge-tunable atomically thin semiconductors. *Nat. Phys.* **13**, 255–261 (2017).
3. Ni, K.-K. et al. A high phase-space-density gas of polar molecules. *Science* **322**, 231–235 (2008).
4. Park, J. W., Will, S. A. & Zwierlein, M. W. Ultracold dipolar gas of fermionic $^{23}Na^{40}K$ molecules in their absolute ground state. *Phys. Rev. Lett.* **114**, 205302 (2015).
5. Rvachov, T. M. et al. Long-lived ultracold molecules with electric and magnetic dipole moments. *Phys. Rev. Lett.* **119**, 143001 (2017).
6. Seeßelberg, F. et al. Modeling the adiabatic creation of ultracold polar $^{23}Na^{40}K$ molecules. *Phys. Rev. A* **97**, 013405 (2018).
7. Yang, H. et al. Observation of magnetically tunable Feshbach resonances in ultracold $^{23}Na^{40}K+^{40}K$ collisions. *Science* **363**, 261–264 (2019).
8. Mak, K. F. et al. Tightly bound trions in monolayer MoS_2. *Nat. Mater.* **12**, 207–211 (2013).
9. De Marco, L. et al. A degenerate Fermi gas of polar molecules. *Science* **363**, 853–856 (2019).
10. Enss, T. & Zwerger, W. Superfluidity near phase separation in Bose–Fermi mixtures. *Eur. Phys. J. B* **68**, 383–389 (2009).
11. Matuszewski, M., Taylor, T. & Kavokin, A. V. Exciton supersolidity in hybrid Bose–Fermi systems. *Phys. Rev. Lett.* **108**, 060401 (2012).
12. Shelykh, I. A., Taylor, T. & Kavokin, A. V. Rotons in a hybrid Bose–Fermi system. *Phys. Rev. Lett.* **105**, 140402 (2010).
13. Cotleț, O., Zeytinoğlu, S., Sigrist, M., Demler, E. & Imamoğlu, A. Superconductivity and other collective phenomena in a hybrid Bose–Fermi mixture formed by a polariton condensate and an electron system in two dimensions. *Phys. Rev. B* **93**, 054510 (2016).
14. Powell, S., Sachdev, S. & Büchler, H. P. Depletion of the Bose–Einstein condensate in Bose–Fermi mixtures. *Phys. Rev. B* **72**, 024534 (2005).
15. Suzuki, K., Miyakawa, T. & Suzuki, T. *p*-wave superfluid and phase separation in atomic Bose–Fermi mixtures. *Phys. Rev. A* **77**, 043629 (2008).
16. Fratini, E. & Pieri, P. Pairing and condensation in a resonant Bose–Fermi mixture. *Phys. Rev. A* **81**, 051605 (2010).
17. Ludwig, D., Floerchinger, S., Moroz, S. & Wetterich, C. Quantum phase transition in Bose–Fermi mixtures. *Phys. Rev. A* **84**, 033629 (2011).
18. Guidini, A., Bertaina, G., Galli, D. E. & Pieri, P. Condensed phase of Bose–Fermi mixtures with a pairing interaction. *Phys. Rev. A* **91**, 023603 (2015).
19. von Milczewski, J., Rose, F. & Schmidt, R. Functional-renormalization-group approach to strongly coupled Bose–Fermi mixtures in two dimensions. *Phys. Rev. A* **105**, 013317 (2022).
20. Kinnunen, J. J., Wu, Z. & Bruun, G. M. Induced *p*-wave pairing in Bose–Fermi mixtures. *Phys. Rev. Lett.* **121**, 253402 (2018).
21. Laussy, F. P., Kavokin, A. V. & Shelykh, I. A. Exciton-polariton mediated superconductivity. *Phys. Rev. Lett.* **104**, 106402 (2010).
22. Hu, M.-G. et al. Bose polarons in the strongly interacting regime. *Phys. Rev. Lett.* **117**, 055301 (2016).

23. Jørgensen, N. B. et al. Observation of attractive and repulsive polarons in a Bose–Einstein condensate. *Phys. Rev. Lett.* **117**, 055302 (2016).
24. Yan, Z. Z., Ni, Y., Robens, C. & Zwierlein, M. W. Bose polarons near quantum criticality. *Science* **368**, 190–194 (2020).
25. Schirotzek, A., Wu, C.-H., Sommer, A. & Zwierlein, M. W. Observation of Fermi polarons in a tunable Fermi liquid of ultracold atoms. *Phys. Rev. Lett.* **102**, 230402 (2009).
26. Koschorreck, M. et al. Attractive and repulsive Fermi polarons in two dimensions. *Nature* **485**, 619–622 (2012).
27. Ness, G. et al. Observation of a smooth polaron-molecule transition in a degenerate Fermi gas. *Phys. Rev. X* **10**, 041019 (2020).
28. Fritsche, I. et al. Stability and breakdown of Fermi polarons in a strongly interacting Fermi–Bose mixture. *Phys. Rev. A* **103**, 053314 (2021).
29. Carr, L. D., DeMille, D., Krems, R. V. & Ye, J. Cold and ultracold molecules: science, technology and applications. *New J. Phys.* **11**, 055049 (2009).
30. Bohn, J. L., Rey, A. M. & Ye, J. Cold molecules: progress in quantum engineering of chemistry and quantum matter. *Science* **357**, 1002–1010 (2017).
31. Marchetti, F. M., Mathy, C. J. M., Huse, D. A. & Parish, M. M. Phase separation and collapse in Bose–Fermi mixtures with a Feshbach resonance. *Phys. Rev. B* **78**, 134517 (2008).
32. Bertaina, G., Fratini, E., Giorgini, S. & Pieri, P. Quantum Monte Carlo study of a resonant Bose–Fermi mixture. *Phys. Rev. Lett.* **110**, 115303 (2013).
33. Zwerger, W. *The BCS-BEC Crossover and the Unitary Fermi Gas* Vol. 836 (Springer, 2011).
34. Haussmann, R., Rantner, W., Cerrito, S. & Zwerger, W. Thermodynamics of the BCS-BEC crossover. *Phys. Rev. A* **75**, 023610 (2007).
35. Houcke, K. V. et al. Feynman diagrams versus Fermi-gas Feynman emulator. *Nat. Phys.* **8**, 366–370 (2012).
36. Schmidt, R. & Enss, T. Excitation spectra and RF response near the polaron-to-molecule transition from the functional renormalization group. *Phys. Rev. A* **83**, 063620 (2011).
37. Parish, M. M., Adlong, H. S., Liu, W. E. & Levinsen, J. Thermodynamic signatures of the polaron-molecule transition in a Fermi gas. *Phys. Rev. A* **103**, 023312 (2021).
38. Viel, A. & Simoni, A. Feshbach resonances and weakly bound molecular states of boson–boson and boson–fermion NaK pairs. *Phys. Rev. A* **93**, 042701 (2016).
39. Chen, X.-Y. et al. Suppression of unitary three-body loss in a degenerate Bose–Fermi mixture. *Phys. Rev. Lett.* **128**, 153401 (2022).
40. Bloom, R. S., Hu, M.-G., Cumby, T. D. & Jin, D. S. Tests of universal three-body physics in an ultracold Bose–Fermi mixture. *Phys. Rev. Lett.* **111**, 105301 (2013).
41. Bause, R. et al. Efficient conversion of closed-channel-dominated feshbach molecules of $^{23}Na^{40}K$ to their absolute ground state. *Phys. Rev. A* **104**, 043321 (2021).
42. Tobias, W. G. Thermalization and sub-Poissonian density fluctuations in a degenerate molecular Fermi gas. *Phys. Rev. Lett.* **124**, 033401 (2020).
43. Zhang, Z., Chen, L., Yao, K.-X. & Chin, C. Transition from an atomic to a molecular Bose–Einstein condensate. *Nature* **592**, 708–711 (2021).
44. Witczak-Krempa, W., Sørensen, E. S. & Sachdev, S. The dynamics of quantum criticality revealed by quantum Monte Carlo and holography. *Nat. Phys.* **10**, 361–366 (2014).
45. Takekoshi, T. et al. Ultracold dense samples of dipolar RbCs molecules in the rovibrational and hyperfine ground state. *Phys. Rev. Lett.* **113**, 205301 (2014).
46. Molony, P. K. et al. Creation of ultracold $^{87}Rb^{133}Cs$ molecules in the rovibrational ground state. *Phys. Rev. Lett.* **113**, 255301 (2014).
47. Guo, M. et al. Creation of an ultracold gas of ground-state dipolar $^{23}Na^{87}Rb$ molecules. *Phys. Rev. Lett.* **116**, 205303 (2016).
48. Voges, K. K. et al. Ultracold gas of bosonic $^{23}Na^{39}K$ ground-state molecules. *Phys. Rev. Lett.* **125**, 083401 (2020).
49. Cairncross, W. B. et al. Assembly of a rovibrational ground state molecule in an optical tweezer. *Phys. Rev. Lett.* **126**, 123402 (2021).
50. Warner, C. et al. Overlapping Bose–Einstein condensates of ^{23}Na and ^{133}Cs. *Phys. Rev. A* **104**, 033302 (2021).
51. Valtolina, G. et al. Dipolar evaporation of reactive molecules to below the Fermi temperature. *Nature* **588**, 239–243 (2020).
52. Li, J.-R. et al. Tuning of dipolar interactions and evaporative cooling in a three-dimensional molecular quantum gas. *Nat. Phys.* **17**, 1144–1148 (2021).
53. Schindewolf, A. et al. Evaporation of microwave-shielded polar molecules to quantum degeneracy. *Nature* **607**, 677–681 (2022).
54. Baranov, M. A., Dalmonte, M., Pupillo, G. & Zoller, P. Condensed matter theory of dipolar quantum gases. *Chem. Rev.* **112**, 5012–5061 (2012).
55. Veljić, V., Pelster, A. & Balaž, A. Stability of quantum degenerate Fermi gases of tilted polar molecules. *Phys. Rev. Res.* **1**, 012009 (2019).
56. Peter, D., Müller, S., Wessel, S. & Büchler, H. P. Anomalous behavior of spin systems with dipolar interactions. *Phys. Rev. Lett.* **109**, 025303 (2012).
57. Gadsbølle, A.-L. & Bruun, G. M. Dipolar fermions in a two-dimensional lattice at nonzero temperature. *Phys. Rev. A* **86**, 033623 (2012).

Methods

Preparing a density-matched degenerate Bose–Fermi mixture

^{23}Na atoms and ^{40}K atoms were loaded into a three-dimensional magneto-optical trap (MOT) from a Zeeman-slower stage for ^{23}Na and a 2D-MOT stage for ^{40}K, followed by grey-molasses cooling for Na atoms on the D_1 line. Both species were transferred into an optically plugged magnetic quadropole trap and cooled by forced radiofrequency evaporation. After evaporation, there were 1.6×10^8 Na atoms and 1.0×10^6 K atoms at a temperature of 6 μK, of which 2×10^7 Na atoms and 6×10^5 K atoms were loaded into an optical trap that transported the mixture from the MOT chamber to a glass cell. This transport trap was formed by two 1,064-nm laser beams intersecting at an angle of 3° to increase axial confinement[58]. After the transport, the mixture was transferred into a crossed optical dipole trap formed by one of the transport beams and an additional 1,550-nm beam (1,550/1,064-nm trap; Fig. 1a). The waists of these two beams in the vertical and horizontal directions were 50 × 100 μm and 50 × 150 μm, respectively. Optical evaporation was performed by exponentially ramping down the beam powers. During the evaporation, a trap formed by two 785-nm beams with waists of 30 × 400 μm and 50 × 50 μm (785-nm trap; Extended Data Fig. 1b) was ramped on. The wavelength of this trap was chosen such that it was closely detuned from the *D* lines of the K atoms, and the polarizabilities of the Feshbach and ground-state molecules were equal[59]. After evaporation, the K atoms underwent two Landau–Zener sweeps for a hyperfine transfer from $|F, m_F\rangle = |9/2, 9/2\rangle$ to $|9/2, -9/2\rangle$, where F is the total atomic angular momentum and m_F is its projection onto the axis of the magnetic field. The Na atoms remained in $|1, 1\rangle$. The first state transfer from $|9/2, 9/2\rangle$ to $|9/2, -7/2\rangle$ was performed at a magnetic field of 74 G, and the second state transfer from $|9/2, -7/2\rangle$ to $|9/2, -9/2\rangle$ was performed at 81 G. The magnetic fields were chosen to minimize changes in the interspecies interaction during the sweeps. After the state preparation, we turned on a magnetic field gradient of 6.4 G cm^{-1} to levitate the Na atoms and K atoms against gravity. Afterwards, the 1,550/1,064-nm trap was ramped down, decompressing mainly the Na atoms and leading to a trap configuration dominated by the 785-nm beams. In this trap configuration, the trap frequencies of the K atoms were approximately three times larger than those of the Na atoms. For the measurements described in the main text, the trapping frequencies in the (x, y, z)-direction were $2\pi \times (72, 90, 187)$ Hz and $2\pi \times (23, 28, 61)$ Hz for the K atoms and Na atoms, respectively. This procedure led to the preparation of a density-matched mixture of 2.3×10^5 ^{40}K atoms at $T = 80$ nK (corresponding to $T/T_F \approx 0.2$ where T_F is the Fermi temperature), and a BEC of 0.8×10^5 ^{23}Na atoms with a condensate fraction of ~60%. In the measurements of the QPT, where we start the association from 1.8×10^5 K atoms, the Fermi wavevector is given by $k_F = 2\pi \times (1.5 \times 10^6)$ m^{-1}.

Feshbach association and preparation for ground-state transfer

To associate Feshbach molecules, we used a series of magnetic-field ramps (Extended Data Fig. 1b). First, the magnetic field was quickly ramped to 78.6 G, followed by the association ramp across the Feshbach resonance at 78.3 G with a ramp speed of 3.5 G ms^{-1}. This slower ramp stopped at 77.8 G, where the formation of Feshbach molecules saturated. To minimize the loss of the Feshbach molecules, we subsequently ramped the magnetic field quickly to 75 G. At this magnetic field, the magnetic moment of the Feshbach molecules reduced by a factor of six compared to the open-channel-dominated Feshbach molecules close to the resonance. We compensated the reduced magnetic moment by increasing the magnetic-field gradient to 40 G cm^{-1} in ~200 μs. This levitated the Feshbach molecules against gravity and, in addition, removed unassociated atoms from the trap due to their larger magnetic moment.

Imperfect timing of the magnetic-field and magnetic-field-gradient ramps resulted in a temporary tilt of the trap, which induced collective oscillations of the molecular cloud. We minimized the collective oscillations by carefully programming the magnetic field and subsequently the magnetic force on the molecules over the course of ~25 ms once the magnetic-field gradient had reached 40 G cm^{-1} (Extended Data Fig. 1c). Once the collective oscillations stopped, the 1,550/1,064-nm trap was compressed within 30 ms. Because the trap was deep enough to hold the molecules without magnetic-field levitation, the magnetic-field gradient was ramped down within 30 ms and the magnetic field was ramped to 72.3 G, where the magnetic moment of the Feshbach molecules vanished. Finally, the stimulated Raman adiabatic passage scheme was used, as described in ref. [4].

Feshbach association at 1,550/1,064 nm

As a comparison to the species-dependent 785-nm trap, we characterized the association of Feshbach molecules in our typical 1,550/1,064-nm trap, where the densities are strongly mismatched as shown in Fig. 1c. The measurement started with 2.9×10^5 K atoms and 1.4×10^5 Na atoms, where the condensed fraction of Na atoms was ~60%. In contrast to the measurements described above, the ramp speed of the magnetic field across the Feshbach resonance was changed to 2.4 G ms^{-1} to maximize the number of Feshbach molecules. The association ramp through the Feshbach resonance was stopped at different magnetic fields, followed by a magnetic-field jump to 72.3 G for Stern–Gerlach detection. Extended Data Fig. 2 shows that only 30,000 Feshbach molecules were associated, resulting in an association efficiency of less than 25%. Around 60% of the Na atoms, primarily Na atoms in the BEC, have been lost due to interspecies collisions. This observation is in contrast to the measurements in the 785-nm trap, where at most 10% of the Na atoms were lost.

Immiscibility and collapse in Bose–Fermi mixtures

Theory[17,31,60,61] and early experiments[62,63] suggest that, for strong interactions, especially close to unitarity, the Bose–Fermi mixture might undergo collapse. However, the timescale for the collapse to occur is on the order of the trapping period. In our experiment, we ramped through the strongly interacting regime on a timescale shorter than the trapping period, prohibiting the collapse to occur. Indeed, our observations show that the Bose–Fermi mixture remains in a metastable state on such experimental timescales, which in turn allows us to explore the physics of the phase diagram shown in Fig. 1a. Specifically, the density increase in a collapse scenario would lead to enhanced interspecies loss, which we do not observe. As a further instability one might also consider immiscibility of the mixture leading to a separation of bosonic and fermionic atoms. Such immiscibility is expected to occur for repulsive interactions between bosons and fermions. We are, however, following the attractive interaction branch of the system and, given the efficient molecule formation we observe, immiscibility, which would be characterized by poor spatial overlap, can be excluded.

Ramp speed of the Feshbach association

We measured the depletion of the condensate fraction as a function of $(k_F a_{BF})^{-1}$ at three different ramp speeds. As shown in Extended Data Fig. 3, the depletion of the condensate coincides for ramp speeds of 1.7 G ms^{-1} and 3.5 G ms^{-1} while showing a shift towards higher $(k_F a_{BF})^{-1}$ for ramp speeds of 9 G ms^{-1}. We attribute the higher residual condensate fraction for the data shown by points to an imperfect trap alignment, which leads to a worse density matching between bosons and fermions.

Heating during the phase transition

We measured the heating of the bosons as a function of $(k_F a_{BF})^{-1}$ at a ramp speed of 3.5 G ms^{-1} by extracting the temperature from the thermal wings of the bosons. As shown in Extended Data Fig. 4, the heating starts around $(k_F a_{BF})^{-1} \approx 0.8$, where the system is close to the predicted transition point. This agrees with the expectation that the system is

excited when the response time of the system becomes slow near the critical point. Interestingly, the heating is mainly in the horizontal direction, along which the confinement is much weaker than along the vertical direction. The anisotropy of the heating and the directional depletion of the BEC (Fig. 2a) indicate involved dynamics of the strongly interacting mixture, which may result from the varying density ratio within the trap and the associated inward movement of the phase boundary. Thus, the quantity deduced from time-of-flight distributions should be regarded rather as an average kinetic energy of the particles, an effective temperature, rather than the actual temperature of the sample. In future work, it would be interesting to resolve the dynamics of the mixture close to the critical point, preferably in a set-up where homogeneous samples can be realized (for example, in a box trap) and high-resolution imaging is available for local detection.

We note that the temperature of the bosons is lower than the global temperature of the fermions (80 nK). We attribute the temperature difference to the reduced interspecies heat contact during the sympathetic cooling once the bosons condense. However, the region of interest where the phase transition takes place is mainly inside the BEC (the centre of the Fermi cloud). In this region the local condensate density is much higher than that of the thermal bosons (Fig. 1b), and the fermions are deeply degenerate, that is, with very few particle–hole excitations compared to the Fermi surface. Therefore our system can be described by an effective local temperature close to zero.

Comparison of NSCT and fRG calculations

The NSCT approach, from which we obtain the condensate depletion at equal density, predicts the polaron-to-molecule transition to occur at $(k_F a_{BF})^{-1} = 1.60$(ref. [18]). For finite boson densities it predicts the phase transition between the polaronic condensate and the molecular phase to take place beyond this value as the boson concentration increases, that is, $(k_F a_{BF})_c^{-1} > 1.60$. Specifically, for the case of balanced densities, $n_B = n_F$, it predicts $(k_F a_{BF})_c^{-1} = 2.02$.

The NSCT approach, however, only takes into account single particle–hole excitations of the Fermi sea[64] and underestimates the modification of the binding energy of molecules inside the many-body environment. Indeed, when applying the NSCT approach[18] to the Fermi–polaron problem at mass balance, one finds the polaron-to-molecule transition to occur at $(k_F a_{BF})_c^{-1} = 1.27$(ref. [65]), while techniques that include higher-order correlations such as fRG[36] and state-of-the-art diagramatic Monte Carlo (QMC)[66,67] predict a value of $(k_F a_{BF})_c^{-1} = 0.90$.

Thus, to obtain a more accurate description of the critical interaction strength for the heteronuclear case considered in this work, we used a fRG scheme, which takes into account an infinite number of particle–hole excitations in the Fermi sea[36]. The resulting polaron and molecule energies are shown in Fig. 1e, yielding a polaron-to-molecule transition at $(k_F a_{BF})^{-1} = 1.16$. As shown in Fig. 1d, we find that the polaron quasiparticle weight obtained in the impurity limit already describes the condensate fraction well, except for its discontinuity at the polaron-to-molecule transition. From investigations of two-component Fermi gases, it is expected that this discontinuity will be smoothed out due to the finite boson density, temperature or combinations thereof[27,37]. Moreover, as explicitly shown in refs. [18,19,27,37] and suggested by mean-field arguments[19], one expects the transition to shift to larger values of $(k_F a_{BF})^{-1}$ as the boson density increases. Hence, the value of $(k_F a_{BF})^{-1} = 1.16$ obtained from the fRG in the impurity limit can be regarded as a lower bound on the actual location of the QPT at $(k_F a_{BF})_c$.

We note that the polaron and molecule energies cross at a rather shallow angle (Fig. 1e). As a result, the underestimation of the molecule energy is the main reason for the difference in the predicted location of the polaron-to-molecule transition in the NSCT and fRG calculations. The quasiparticle weight is, in contrast, less affected, and, as shown in Extended Data Fig. 5, both approaches yield similar results for the quasiparticle weight of a bosonic impurity. Based on this finding, NSCT theory can also be expected to give a reliable prediction for the condensate fraction at finite boson density[18].

Projection of polaronic states onto deeply bound molecules

As is evident from Fig. 2b, we detect a finite number of Feshbach molecules even before the phase transition. This can be understood from the fact that the rapid ramp to 72.3 G projects the system onto deeply bound molecules. As a result, short-distance pairing correlations between bosons and fermions are effectively measured before the phase transition. However, once the phase transition is crossed in the initial magnetic-field ramp, all bosons are bound into weakly bound molecules in an adiabatic fashion. In that case, the weakly bound Feshbach molecules are transferred into deeply bound states by the subsequent rapid magnetic-field ramp.

Here we demonstrate that a simple Fermi–polaron wavefunction indeed overlaps with deeply bound molecules when a projection measurement, as described in the main text, is performed. Similar to the calculations performed in ref. [68], we define the molecule number operator as

$$\hat{N}_{\mathrm{Mol}} = \sum_{\mathbf{mlk}} c^{\dagger}_{\mathbf{m}+\mathbf{k}} d^{\dagger}_{-\mathbf{k}} \phi_{\mathbf{m}}(\mathbf{k}) \phi^{*}_{\mathbf{m}}(\mathbf{l}) d_{-\mathbf{l}} c_{\mathbf{m}+\mathbf{k}}. \tag{1}$$

Here, $d_{\mathbf{q}}$ and $c_{\mathbf{q}}$ are the fermionic and bosonic annihilation operators, respectively, and $\phi_{\mathbf{p}}(\mathbf{k})$ denotes the wavefunction of the molecule in vacuum at centre-of-mass momentum $\mathbf{p}$. We approximate it with the form valid for an attractive contact interaction potential:

$$\tilde{\phi}_{\mathbf{p}}(\mathbf{k}) = \frac{1}{E_b + \frac{\alpha+1}{2m\alpha}\left(\mathbf{k} + \frac{\alpha}{1+\alpha}\mathbf{p}\right)^2}, \tag{2}$$

$$\phi_{\mathbf{p}}(\mathbf{k}) = \frac{\tilde{\phi}_{\mathbf{p}}(\mathbf{k})}{\sqrt{\sum_{\mathbf{l}} |\tilde{\phi}_{\mathbf{p}}(\mathbf{l})|^2}}. \tag{3}$$

Here, E_b denotes the energy of the molecule at $\mathbf{p} = 0$, m denotes the mass of the fermions, and α is given by the ratio of the bosonic and the fermionic mass.

The operator $\hat{N}_{\mathrm{Mol}}$ measures the number of projected molecules with respect to the Chevy Ansatz[69] for the Fermi polaron

$$|\,\mathrm{Pol}\,\rangle = \alpha_0 d^{\dagger}_0 |\,\mathrm{FS}(N)\,\rangle + \sum_{\mathbf{kq}} \alpha_{\mathbf{kq}} d^{\dagger}_{\mathbf{q}-\mathbf{k}} c^{\dagger}_{\mathbf{k}} c_{\mathbf{q}} |\,\mathrm{FS}(N)\,\rangle \tag{4}$$

as $N_{\mathrm{Mol}} = \langle\,\mathrm{Pol}\,|\,\hat{N}_{\mathrm{Mol}}\,|\,\mathrm{Pol}\,\rangle$ Here, α_0 and $\alpha_{\mathbf{kq}}$ denote variational parameters and $|\,\mathrm{FS}(N)\,\rangle$ denotes a Fermi sea containing N fermions.

The resulting fractions are shown in Extended Data Fig. 6 for a mass ratio of $\alpha = 23/40$ and different values of E_b. For the binding energies shown, it can be seen that with increasing $(k_F a_{BF})^{-1}$, the molecule fraction increases, with the fraction becoming smaller as E_b increases. This shows that, although the polaron is by no means a molecular state, it still features pairing correlations that will lead to a finite overlap with deeply bound molecules. Note that when the transition to the molecular phase is reached, in our experimental procedure the associated weakly bound molecules will be transferred nearly adiabatically to the more deeply bound molecules approximately described by equation (2). Accordingly, the number of observed molecules would approximately saturate (in the absence of losses). However, because, during the final part of the initial ramp, excess bosons undergo lossy collisions with the molecules, the number of molecules will be further reduced and it is thus expected that the number of observed molecules will in fact be maximized at the transition using our experimental procedure.

Two-body loss of Feshbach and ground-state molecules

We measured the two-body loss rate of Feshbach and ground-state molecules. For Feshbach molecules, the loss measurement was performed after the 100-ms holding time, during which collective oscillations are dampened out and the 1,550/1,064-nm trap has been compressed. The loss measurement of ground-state molecules was performed immediately after the transfer into the ground state, followed by a removal of the residual Feshbach molecules by resonant light pulses. The trapping frequency for Feshbach and ground-state molecules was $(\omega_x, \omega_y, \omega_z) = 2\pi \times (71, 99, 234)$ Hz, because we increased the power of the 1,550/1,064-nm trap to compensate for the change of polarizabilities between the Feshbach and ground-state molecules.

We started from a density-dependent two-body loss model with heating:

$$\frac{\mathrm{d}n}{\mathrm{d}t} = -\beta n^2 - \frac{3}{2}\frac{n}{T}\frac{\mathrm{d}T}{\mathrm{d}t}, \tag{5}$$

where n represents the average density and T the temperature of the molecular sample. The two-body loss coefficient is expected to scale linearly with temperature, as was experimentally confirmed for fermionic ground-state molecules[70,71]. With this knowledge, we defined the temperature-independent loss coefficient $b = \beta/T$, where we obtain the temperature T by fitting Fermi–Dirac distribution to the molecular clouds. In a first step, we fitted the temperature with a linear-heating model $T_{\mathrm{lin}}(t) = T_0 + ht$, where T_0 is the initial temperature and h the heating rate. Using this linear model for heating, we solve equation (5) and obtain[9]

$$n(t) = \frac{n_0 h T_0^{3/2}}{T_{\mathrm{lin}}(t)\left(2n_0 T_0^2(\sqrt{T_0} - \sqrt{T_{\mathrm{lin}}(t)})b + h(\sqrt{T_{\mathrm{lin}}(t)} + 2n_0 t T_0^{3/2} b)\right)}, \tag{6}$$

where n_0 describes the initial density of the sample. We fit equation (6) to our data with n_0 and b as free parameters. In analogy to ref. [9], we extracted the density of the sample by approximating the degenerate Fermi gas as a classical gas at a temperature of T_{cl}. We obtain T_{cl} by fitting a Gaussian distribution to the time-of-flight images. The average in situ density of the classical gas is given by

$$n(T_{\mathrm{cl}}) = \frac{N}{8\pi^{3/2}}\bar{\omega}^3\left(\frac{k_{\mathrm{B}}T_{\mathrm{cl}}}{m}\right)^{-3/2}, \tag{7}$$

where $\bar{\omega}$ is the geometric average of the trapping frequency, and the classical temperature T_{cl} accounts for the Fermi pressure as well as the kinetic energy of the sample, thus overestimating the actual temperature. Still, this effective model allows us to determine the density of the sample, even in the degenerate regime, with the least assumptions with respect to the loss and whether the sample is in thermal equilibrium. The accuracy in determining the density for degenerate Fermi samples using a Gaussian distribution instead of a Fermi–Dirac distribution was checked numerically in ref. [72]. This shows that the error is negligible for Fermi gases at temperatures as low as $0.2T_{\mathrm{F}}$.

Extended Data Fig. 7 shows the loss measurement of the Feshbach and ground-state molecules. For Feshbach molecules we get $b_{\mathrm{FB}} = 3.8(5) \times 10^{-12}\ \mathrm{cm^3\,\mu K^{-1}\,s^{-1}}$ and for ground-state molecules we get $b_{\mathrm{GS}} = 4.8(6) \times 10^{-11}\ \mathrm{cm^3\,\mu K^{-1}\,s^{-1}}$.

Error bars for the measurements

The error bars in $(k_{\mathrm{F}}a_{\mathrm{BF}})^{-1}$ in Figs. 1d and 2 result from the magnetic field uncertainty of 15 mG and an error of 10% in the average trapping frequency. The vertical error bars in Figs. 1d and 2, as well as Extended Data Figs. 2, 3 and 6, are the standard deviation of three to five measurements.

Data availability

The experimental data that support the findings of this study are available from the corresponding author upon reasonable request.

Code availability

All relevant codes are available from the corresponding author upon reasonable request.

References

58. Gross, C., Gan, H. C. J. & Dieckmann, K. All-optical production and transport of a large ^{6}Li quantum gas in a crossed optical dipole trap. *Phys. Rev. A* **93**, 053424 (2016).
59. Vexiau, R. et al. Dynamic dipole polarizabilities of heteronuclear alkali dimers: optical response, trapping and control of ultracold molecules. *Int. Rev. Phys. Chem.* **36**, 709–750 (2017).
60. Mølmer, K. Bose condensates and Fermi gases at zero temperature. *Phys. Rev. Lett.* **80**, 1804–1807 (1998).
61. Yu, Z.-Q., Zhang, S. & Zhai, H. Stability condition of a strongly interacting boson–fermion mixture across an interspecies Feshbach resonance. *Phys. Rev. A* **83**, 041603 (2011).
62. Zaccanti, M. et al. Control of the interaction in a Fermi–Bose mixture. *Phys. Rev. A* **74**, 041605 (2006).
63. Ospelkaus, C., Ospelkaus, S., Sengstock, K. & Bongs, K. Interaction-driven dynamics of ^{40}K–^{87}Rb fermion–boson gas mixtures in the large-particle-number limit. *Phys. Rev. Lett.* **96**, 020401 (2006).
64. Lobo, C., Recati, A., Giorgini, S. & Stringari, S. Normal state of a polarized Fermi gas at unitarity. *Phys. Rev. Lett.* **97**, 200403 (2006).
65. Punk, M., Dumitrescu, P. T. & Zwerger, W. Polaron-to-molecule transition in a strongly imbalanced Fermi gas. *Phys. Rev. A* **80**, 053605 (2009).
66. Prokof'ev, N. & Svistunov, B. Fermi-polaron problem: diagrammatic Monte Carlo method for divergent sign-alternating series. *Phys. Rev. B* **77**, 020408 (2008).
67. Prokof'ev, N. V. & Svistunov, B. V. Bold diagrammatic Monte Carlo: a generic sign-problem tolerant technique for polaron models and possibly interacting many-body problems. *Phys. Rev. B* **77**, 125101 (2008).
68. Pini, M., Pieri, P., Jäger, M., Denschlag, J. H. & Strinati, G. C. Pair correlations in the normal phase of an attractive Fermi gas. *New J. Phys.* **22**, 083008 (2020).
69. Chevy, F. Universal phase diagram of a strongly interacting Fermi gas with unbalanced spin populations. *Phys. Rev. A* **74**, 063628 (2006).
70. Ospelkaus, S. et al. Quantum-state controlled chemical reactions of ultracold potassium-rubidium molecules. *Science* **327**, 853–857 (2010).
71. Bause, R. et al. Collisions of ultracold molecules in bright and dark optical dipole traps. *Phys. Rev. Res.* **3**, 033013 (2021).
72. DeMarco, B. *Quantum Behavior of an Atomic Fermi Gas*. PhD thesis, Univ. Colorado (2001).

Acknowledgements

We thank P. Pieri for stimulating discussions and providing calculations of the condensate fraction for an equal-density mixture, T. Shi for stimulating discussions, and X. Li and T. Hilker for insightful comments on our paper. We thank the previous members of the MPQ NaK Lab, especially C. Gohle, for their contributions to the experimental apparatus. We acknowledge funding support by the Deutsche Forschungsgemeinschaft under Germany's Excellence Strategy – EXC-2111 – 390814868 (the Munich Center for Quantum Science and Technology) and under grant no. FOR 2247. The experimental team

acknowledges support from the Max Planck Society and the European Union (PASQuanS grant no. 817482). R.S. acknowledges funding by the Deutsche Forschungsgemeinschaft under Germany's Excellence Strategy – EXC-2181/1-390900948 (the Heidelberg STRUCTURES Excellence Cluster). J.v.M. is supported by a fellowship of the International Max Planck Research School for Quantum Science and Technology (IMPRS-QST). A.S. acknowledges funding from the Max Planck Harvard Research Center for Quantum Optics.

Author contributions

All authors contributed substantially to the work presented in this paper. M.D. and X.-Y.C. carried out the experiments and, together with A.S. and R.B., they maintained and improved the experimental set-up. M.D. analysed the data. J.v.M. and R.S. performed the theoretical calculations. R.S., I.B. and X.-Y.L. supervised the study. All authors worked on interpretation of the data and contributed to the final paper.

Funding

Open access funding provided by Max Planck Society.

Competing interests

The authors declare no competing interests.

Additional information

Extended data is available for this paper at https://doi.org/10.1038/s41567-023-01948-1.

Supplementary information The online version contains supplementary material available at https://doi.org/10.1038/s41567-023-01948-1.

Correspondence and requests for materials should be addressed to Xin-Yu Luo.

Peer review information *Nature Physics* thanks Pietro Massignan and the other, anonymous, reviewer(s) for their contribution to the peer review of this work.

https://doi.org/10.1038/s41567-023-01948-1

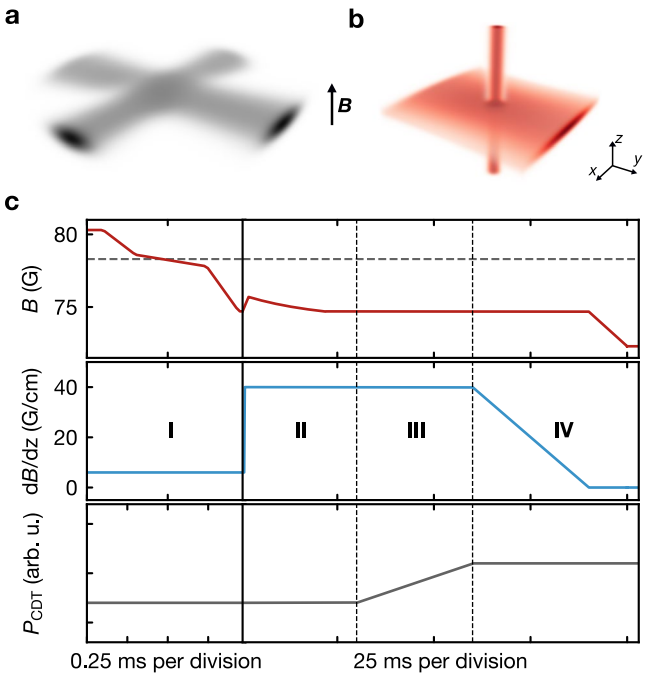

Extended Data Fig. 1 | Trap configurations and sequence for molecule association. a, Trap configuration of the 1550/1064-nm trap and **b,** the 785-nm trap. The magnetic field and its gradient are along the vertical direction (z-direction). **c**, Typical timing sequence for the association of ground-state molecules showing ramps of the magnetic field (red), its gradient (blue) and the power of the 1550/1064-nm trap (gray). I. Association of Feshbach molecules by three-staged magnetic field ramp. II. Removal of unassociated atoms. III. Compression of the 1550/1064-nm trap while the power of the 785-nm trap remains unchanged. IV. Removal of the levitation gradient for subsequent STIRAP pulses. The black vertical solid and dashed lines separate different stages of the sequence. The horizontal gray dashed line marks the Feshbach resonance at 78.3 G.

https://doi.org/10.1038/s41567-023-01948-1

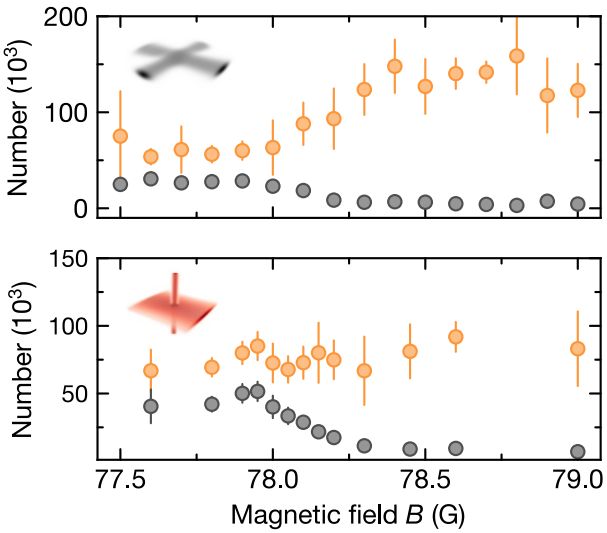

Extended Data Fig. 2 | Feshbach association in the (a) 1550/1064-nm and (b) 785-nm trap. Number of Feshbach molecules (gray) and the sum of associated and unassociated sodium atoms (orange).

https://doi.org/10.1038/s41567-023-01948-1

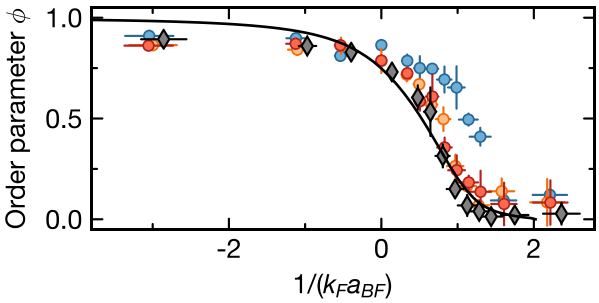

Extended Data Fig. 3 | Feshbach association at various ramp speeds. Order parameter ϕ as a function of $(k_F a_{BF})^{-1}$ at ramp speeds of 1.7 G/ms (red points), 3.5 G/ms (orange points) and 9 G/ms (blue points). In addition, we show the data from the main text at the ramp speed of 3.5 G/ms for $\tilde{n}_B/\tilde{n}_F = 1.3$ (grey diamonds).

https://doi.org/10.1038/s41567-023-01948-1

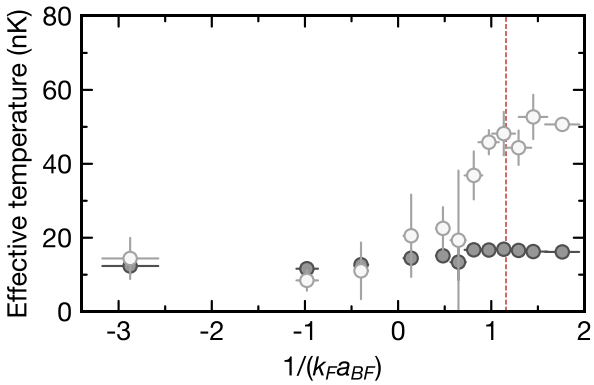

Extended Data Fig. 4 | Effective temperature of the bosons extracted from the thermal wings as a function of the interaction strength in the vertical (dark gray) and horizontal direction (light gray). The predicted polaron-to-molecule according to the fRG calculation at $(k_F a_{BF})^{-1} = 1.16$ is indicated by the red dashed line.

https://doi.org/10.1038/s41567-023-01948-1

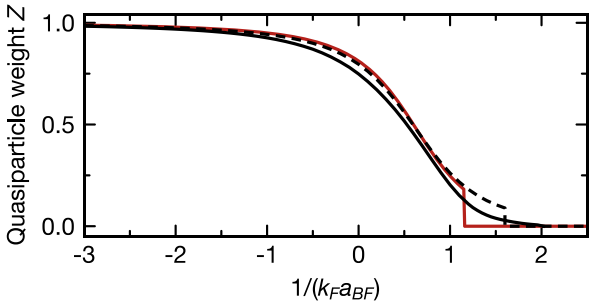

Extended Data Fig. 5 | Impurity quasiparticle weight in the Fermi polaron problem for $\alpha = 23/40$. The quasiparticle weight of the impurity as a function of the interaction strength is shown as obtained from the fRG (red, solid) and the NSCT approach (black, dashed). While both methods yield similar results they differ in the prediction of the point where the polaron-to-molecule transitions occurs, beyond which the occupied quasiparticle weight drops to zero. To indicate the effect of finite boson density, the condensate fraction of the mixture computed in NSCT is shown for $n_B = n_F$ (black solid, also shown in Fig. 1d).

https://doi.org/10.1038/s41567-023-01948-1

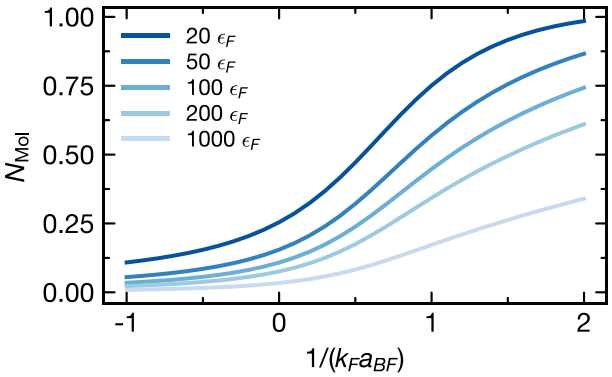

Extended Data Fig. 6 | Number of projected molecules. The projected molecule fraction N_{Mol} obtained from the Fermi polaron state within the Chevy Ansatz[69] is shown as a function of the interaction parameter $(k_F a_{BF})^{-1}$ for different binding energies of the deeply bound molecule.

https://doi.org/10.1038/s41567-023-01948-1

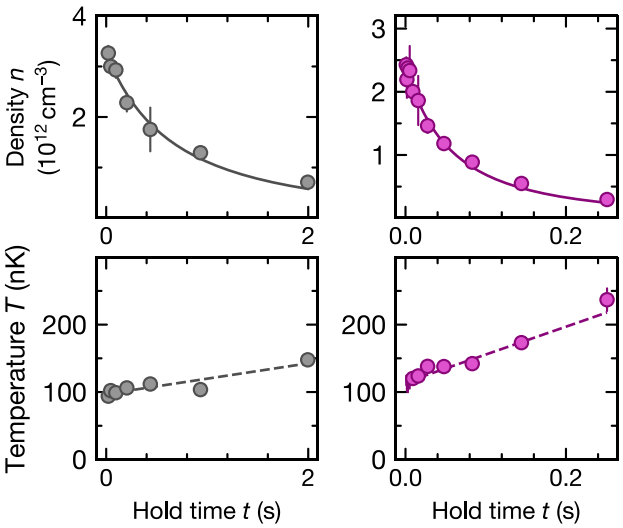

Extended Data Fig. 7 | Lifetime of NaK* Feshbach (left panel) and NaK ground-state molecules (right panel). The upper panel figure shows the average density n of the Feshbach molecules (gray points) and ground-state molecules (purple points) as a function of holding time. The data is fitted with Eq. (6). The result of the fits are plotted as solid lines. The error bars are statistical errors derived from the atom number fluctuations. For the fitting procedure we only consider data points where the molecule number is larger than 1×10^4. The lower panel shows the temperature of the Feshbach molecules (gray points) and the ground-state molecules (purple points) as a function of the holding time extracted from Fermi-Dirac distribution fits. The dashed lines represent the linear fit of the temperature.